

Effect of hole doping on the electronic structure of $\text{Nd}_{1-x}\text{Sr}_x\text{TiO}_3$

S. W. Robey

National Institute of Standards and Technology, Gaithersburg, Maryland, 20899

V. E. Henrich

Department of Applied Physics, Yale University, New Haven, Connecticut 06520

C. Eylem and B. W. Eichhorn

Center for Superconductivity Research, Department of Chemistry and Biochemistry, University of Maryland, College Park, Maryland 20742

(Received 4 April 1995)

Photoelectron spectroscopy has been employed to follow the development of the electronic structure in $\text{Nd}_{1-x}\text{Sr}_x\text{TiO}_3$ as a function of x . Resonant effects at the Ti 3*p* threshold were used to highlight Ti 3*d* contributions in the valence bands. Particular attention is focused on Ti 3*d* intensity within ~ 3 eV of the Fermi level (E_F). The total intensity in this region is found to correlate linearly with composition, as expected. Changes in the shape of this spectral structure are discussed in terms of the one-electron spectral function. For $x < 0.25$ (insulating or semiconducting compositions), only incoherent intensity associated with the lower Hubbard band is present. Additional intensity, attributed to a coherent quasiparticle contribution, appears at the composition of the metal-insulator transition $x \sim 0.25$. The relative intensities of these two components are determined as a function of x . Ti 3*d* intensity also occurs in the higher binding-energy region of the predominantly O 2*p* band due to Ti 3*d*-O 2*p* hybridization. Composition-dependent changes in this region are analyzed in order to determine changes in the Ti 3*d*-O 2*p* hybridization with composition and structure.

I. INTRODUCTION

In this paper we present the results of an ultraviolet photoelectron spectroscopy (UPS) investigation of modifications to the electronic structure in the mixed oxide system $\text{Nd}_{1-x}\text{Sr}_x\text{TiO}_3$ as a function of x . Interest in this oxide stems from the desire to understand factors controlling the composition-dependent metal-insulator transition in highly correlated systems. One goal is to examine the development of the one-particle spectral function, obtained from photoelectron spectroscopy measurements, as the Mott-Hubbard insulator NdTiO_3 is hole doped through a metal-insulator transition. The one-particle spectral function is, in general, comprised of coherent and incoherent components, with relative intensities that are an indication of the importance of correlation effects.¹

Interest in this topic was stimulated by a recent study of transition-metal oxides with varying values of U/W , where U is the effective electron-electron correlation energy and W is the bandwidth.² Emission from the partially localized metal d states was found to be composed of two contributions, identified with the coherent and incoherent portions of the spectral function, that varied in relative intensity as a function of U/W . An analogous behavior has been observed in the Ti 3*d* emission from $\text{Nd}_{1-x}\text{Ba}_x\text{TiO}_3$, which is also a case where variation of x leads to a composition-driven metal-insulator transition.³ Only incoherent intensity was present for insulating compositions, but both coherent and incoherent intensities were observed in the metallic regime. That study was limited in the number of compositions examined, and it

was not possible to follow the changes in any detail across the metal-insulator transition. Most other previous studies of composition-controlled metal-insulator transitions in related materials⁴⁻⁹ have focused primarily on describing the overall intensity changes with doping in a one-electron density-of-states framework. Many-body effects were considered in a study of the composition dependence in $\text{La}_{1-x}\text{Sr}_x\text{TiO}_3$, but no changes were observed in the spectral function due to difficulties in controlling the oxygen stoichiometry.¹⁰ The present work provides a detailed description of the development of the spectral function across the metal-insulator transition using a series of carefully characterized compounds.

We also consider changes in the Ti 3*d*-O 2*p* hybridization as a function of composition. The degree of hybridization is intimately connected with the influence of electron-electron correlation on the one-particle spectral function because the relative importance of correlation effects depends on the ratio, U/W , and Ti-O hybridization is the primary factor influencing the Ti 3*d* bandwidth. Inoue *et al.*¹¹ recently performed a detailed investigation of the one-particle spectral function in the d^1 system, $\text{Ca}_{1-x}\text{Sr}_x\text{VO}_3$. That work did not provide details of the behavior around a metal-insulator transition, but it did produce a picture of the influence of the bandwidth W on the spectral function. The present work is complementary, and together these two studies provide interesting insights into correlation effects in transition-metal oxides.

Section II provides a brief description of experimental procedures. This is followed in Sec. III with the presentation of photoemission data, highlighting modifications

to the spectra as a function of composition. Section IV then uses these results in a discussion of the total Ti 3*d* band filling, the Ti 3*d*-O 2*p* hybridization, and the Ti 3*d* spectral function near E_F as a function of composition. A summary of the main findings is provided in Sec. V.

II. EXPERIMENT

The system $\text{Nd}_{1-x}\text{Sr}_x\text{TiO}_3$ was chosen for several reasons. The Ti 3*d* states that are filled by electron donation from Nd cations are well separated from the O 2*p* states, making it easy to follow changes in the Ti 3*d* emission across the metal-insulator transition. Also, the photoemission final states are either d^0 or d^1 , so that consideration of multiplet effects in the Ti 3*d* structure is unnecessary. Finally, the metal-insulator transition occurs for a Sr fraction, $x=0.25$, making both the insulating and metallic regimes easily accessible.

Details of the sample synthesis and characterization are provided elsewhere,¹² and only a brief description will be given here. A series of ten polycrystalline samples was synthesized by dc arc melting, with compositions ranging from $x=0$ to 0.9: $x=0.05, 0.10, 0.20, 0.25, 0.30, 0.50, 0.60, 0.67, 0.80,$ and 0.90 . Care was taken to ensure the proper oxygen content using thermogravimetric analysis (TGA). Two samples were produced for each composition, one for characterization and one for photoemission studies. With increasing x , transport measurements indicated a semiconductor-to-metal transition at $x\sim 0.20-0.25$. Another transition, back to insulating behavior, occurs close to $x=1$, but this will not be considered here. X-ray-diffraction data were interpreted in terms of an orthorhombic structure for $x=0$ to ~ 0.60 and a cubic perovskite structure for $x > 0.60$.¹²

Angle-integrated photoemission measurements were performed using a double-pass cylindrical mirror analyzer (CMA). The ultrahigh-vacuum (UHV) analysis chamber was located on beamline 8 at the NIST SURF II storage ring. A toroidal-grating monochromator provided photons in the energy range from 20 to 150 eV. The overall energy resolution (monochromator plus electron energy analyzer) was approximately 0.5 eV at a photon energy of 48 eV. The Fermi level of a gold foil was used as the reference for binding energies. The uncertainty in the position of the spectra with respect to the Fermi energy is less than 0.1 eV.

Sample surfaces were prepared by scraping in UHV with a diamond file. Good surface quality was ensured by monitoring the contamination-induced intensity at a binding energy of ~ 11 eV.¹³ A well-defined peak is readily visible in this region well before there are any intensity changes in the structure from a freshly prepared surface. Thus only spectra that exhibited no detectable evidence of this peak were used. Fresh surfaces were prepared frequently and monitored before and after data collection for contamination. The reproducibility of the spectra for different scrapes was excellent, and the results presented below were obtained after averaging data from several separate surface preparations to improve the signal-to-noise ratio.

III. RESULTS

Photoemission spectra for each composition were obtained using excitation energies both below and above the threshold for Ti 3*p* excitation ($\sim 40-41$ eV). Resonant effects¹⁴ produce enhanced intensity from Ti 3*d* contributions to the valence bands for spectra obtained with 48-eV excitation (above the Ti 3*p* threshold). This is evident in Fig. 1(a), which provides a comparison of raw data from $\text{Nd}_{0.95}\text{Sr}_{0.05}\text{TiO}_3$ obtained with 35- and 48-eV excitations. Strong resonant enhancement of the Ti 3*d* states at binding energies from E_F to ~ 3 eV is clearly visible. These states arise from the substitution of Nd for Sr, leading to a change in the Ti formal valence from SrTiO_3 (formally d^0) to NdTiO_3 (formally d^1). The prominent structure located between $\sim 4-$ and 10 -eV binding energy is due to predominantly O 2*p* states. The Nd 4*f* levels do not participate in bonding and are too weak in intensity to significantly influence our discussion below. For simplicity this structure will be referred to below as the O 2*p* photoemission, even though enhanced intensity at ~ 7.5 eV in the 48-eV spectrum indicates Ti 3*d* contributions there as well.

The Ti 3*d* contributions can most clearly be seen in Fig. 1(b), where a difference curve (48-eV spectrum minus 35-eV spectrum) is displayed. To produce this curve, the raw spectra were processed by first subtracting a constant background fitted to the intensity above the

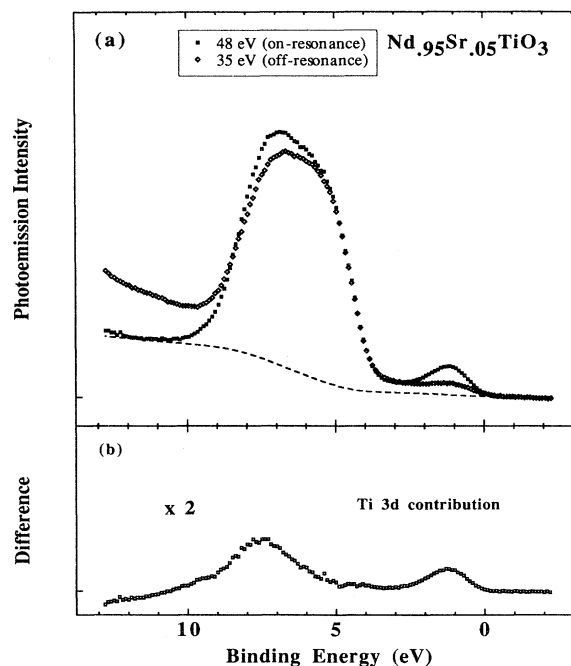


FIG. 1. (a) Photoemission data both before the Ti 3*p* threshold (35 eV) and after the threshold (48 eV). Resonant enhancements of Ti 3*d* contributions are evident at binding energies of ~ 1.5 and 7.5 eV. The dashed line gives the function used to remove the background due to inelastic processes. (b) Difference curve (after background subtraction) derived from data in part (a).

Fermi level to account for the effects of higher-order light. An integral-type function, to account for the inelastic background,¹⁵ was then removed. An example of this integral background is provided by the dotted curve in Fig. 1(a). After background subtraction, the two spectra were normalized to each other for binding energies from about 4 to 5 eV. The states in this region are primarily of nonbonding O 2*p* character, and are thus not influenced by the resonance at the Ti 3*d* edge. This normalization compensates for the change in the O 2*p* cross section with photon energy, leaving only the effect on the Ti 3*d* contribution. The Ti 3*d* intensity at 6–9 eV arises from the hybridization between Ti 3*d* and O 2*p* states. Similar hybridization has been observed in TiO₂,¹⁶ BaTiO₃,¹⁷ and SrTiO₃.¹⁸ The origin of the intensity near E_F was discussed above.

Several spectral changes are observed as a function of composition. These changes are illustrated in Fig. 2, which compares spectra from two representative compositions, $x=0.6$ and $x=0.05$. Composition-dependent modifications are seen to occur in both regions that contain significant Ti 3*d* intensity. The most striking effect is near E_F , where the increased Ti 3*d* occupation with increasing Nd concentration is evident. There are also changes in the spectral shape of the Ti 3*d* intensity near E_F , not clearly evident in Fig. 2, that will provide the basis for our discussion of the development of the one-particle spectral function with composition. Finally, changes in the shape of the O 2*p* band are observed, indicating changes in the Ti-O hybridization. We will consider each of these effects in turn.

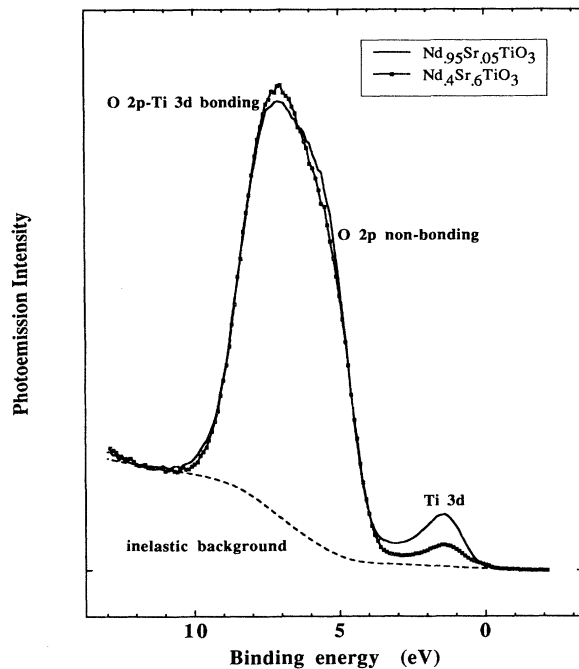


FIG. 2. Comparison of photoemission data obtained with 48-eV excitation for two compositions, Nd_{0.95}Sr_{0.05}TiO₃ (insulating) and Nd_{0.4}Sr_{0.6}TiO₃ (metallic).

A. Total Ti 3*d* intensity near E_F

For NdTiO₃ all Ti ions are formally Ti³⁺, with one 3*d* electron on each Ti ion; its Ti 3*d* orbital population should therefore be 1. For SrTiO₃, formally there are no Ti 3*d* electrons. Therefore, x represents both the Sr fraction and the increase in the number of holes in the Ti 3*d* band with composition, from NdTiO₃. The intensity from the Ti 3*d* states near E_F should provide a measure of this change in Ti 3*d* band filling, a fundamental parameter in characterizing the properties of Nd_{1-x}Sr_xTiO₃. The variation of the Ti 3*d* intensity with composition was determined from the data by integrating the area under the UPS spectra for energies from E_F to about 3-eV binding energy. The intensity from the O 2*p* band was removed by modeling its upper edge with a single Gaussian function for each composition, after removal of the inelastic background as described above. The O 2*p* intensity extending into the region with significant intensity for the Ti 3*d* states is small, so the results are insensitive to the functional form chosen to model the O 2*p* contribution. A Gaussian function provided a good approximation to the intensity in the region from E_F to ~ 3 eV for Nd_{0.1}Sr_{0.9}TiO₃ samples that were exposed to about 10³ L of oxygen to almost completely remove the Ti 3*d* intensity in this region. Figure 3 plots the resulting Ti/3*d* intensity, normalized to the total O 2*p* valence-band emission, as a function of composition. (The total O 2*p* valence-band emission was determined by subtracting the total Ti 3*d* emission intensity, as determined above, from the integral under the entire UPS spectrum from above E_F to a

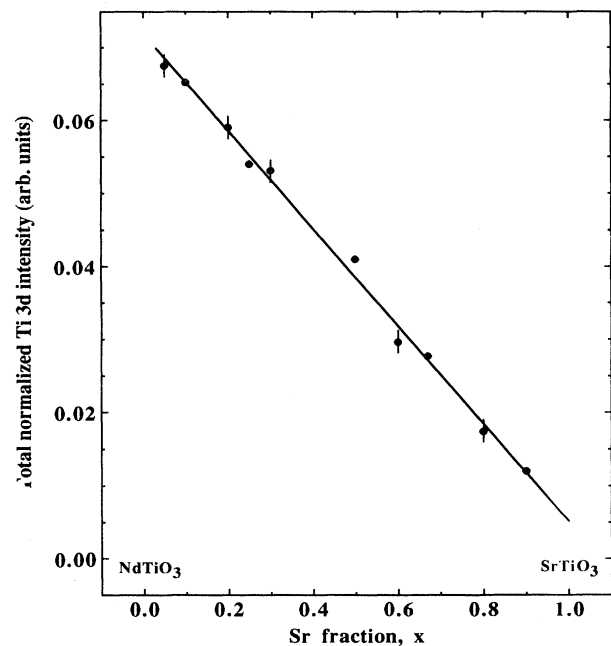


FIG. 3. Integrated intensity in the Ti 3*d* emission between binding energies of 3 eV to E_F (normalized to the total O 2*p* intensity) in Nd_{1-x}Sr_xTiO₃ as a function of Sr fraction x .

point below the O 2*p* band.) Results similar to those in Fig. 3 were also obtained for UPS spectra excited with $h\nu=35$ eV photons; however, the Ti 3*d* emission is much smaller in that case since the photon energy lies significantly below the Ti 3*p*→3*d* optical-absorption threshold, and the photoemission is thus not resonantly enhanced.

The total Ti 3*d* emission (normalized to the total O 2*p* intensity) decreases smoothly with x , as shown in Fig. 3. The solid line is a linear least-squares fit to the data points. It does not extrapolate exactly to zero at $x=1$, presumably due to systematic errors in extracting the intensities. A slight error is introduced in the 48-eV data from the normalization to the O 2*p* intensity. Although, ideally, there is no change in the O 2*p* stoichiometry as a function of composition (hence the motivation for this normalization), small changes in Ti 3*d*-O 2*p* hybridization, to be discussed below, produce changes in the total O 2*p* intensity with composition due to slightly different resonant enhancements. This change in hybridization is a small effect, however, contributing errors of $\sim 2-3\%$. The most important aspect of the data in Fig. 3 is the good linear correlation between Ti 3*d* band-gap intensity and composition. This result indicates that the band filling varies smoothly and linearly throughout the composition range, even though the system goes through structural changes, and the metal-insulator transition also provides a consistency check on the data analysis procedures.

B. Spectral changes in the Ti 3*d* intensity near E_F

In addition to the linear change in Ti 3*d* intensity near E_F with x illustrated above, more subtle modifications to the spectra also occur in this region. These changes are illustrated in Fig. 4, which shows the intensity in the Ti 3*d* region for several representative compositions. The spectra have been normalized at the maximum of the 3*d* peak to emphasize changes in the spectral shape. It can be seen that semiconducting compositions exhibit only a broad Gaussian peak centered at ~ 1.4 eV. This structure cannot be explained in a one-electron picture and is attributed to incoherent emission which develops into the lower Hubbard band.^{2,13} This feature constitutes the major contribution for all compositions, and its position and width are independent of stoichiometry. For metallic compositions ($x > 0.25$), however, an additional structure appears at the Fermi level. This structure increases in intensity rapidly from $x=0.25$ to 0.30. Data near E_F for the entire composition range are plotted in the inset in Fig. 4 to indicate more clearly the abrupt increase in Fermi edge emission that occurs between $x=0.25$ and 0.30, compared to the more gradual changes observed for $x=0.30-0.90$. As in Ref. 2, this contribution is identified as arising from the development of a quasiparticle, or coherent, component of the one-electron spectral function.

The development of the spectral function with composition was studied in more detail by decomposing it into coherent, I_{coh} , and incoherent, I_{incoh} , contributions. This decomposition was performed in two ways. One method

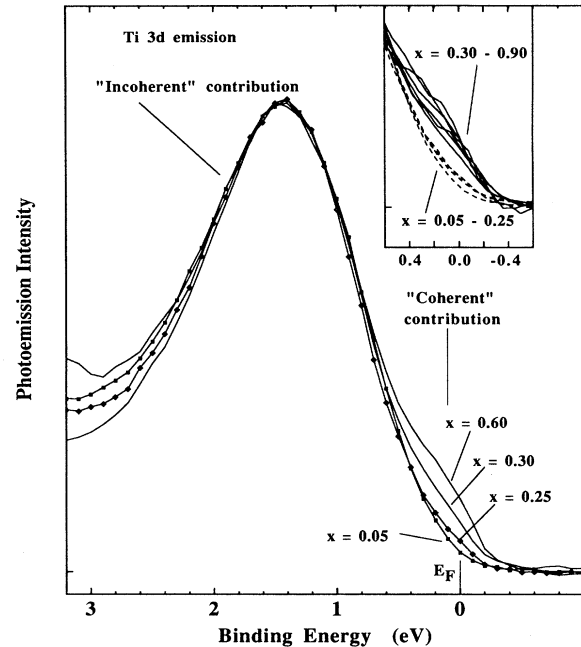


FIG. 4. Comparison of the spectral shape of the Ti 3*d* emission near E_F for several compositions. Note the rapid increase in intensity in the coherent contribution near E_F between compositions of $x=0.25$ and 0.30, compared to the more gradual change from $x=0.30-0.60$. The inset includes data from all compositions to indicate the abrupt increase at $x=0.25$ more clearly.

consisted of fitting the incoherent emission to a single Gaussian, after removal of the O 2*p* and background contributions as described above, and then subtracting that Gaussian from the measured spectrum and integrating the resulting difference spectrum to obtain the coherent contribution. An alternative method involved fitting Gaussian functions to both the coherent and incoherent features and then using the area in the weak Gaussian near E_F to represent the coherent intensity. The values obtained by these two methods were nearly identical. The results of this decomposition are displayed in Fig. 5 as a function of hole doping, which, as indicated above, is equivalent to the Sr fraction x . The total coherent intensity (normalized to the O 2*p* intensity) is plotted in Fig. 5(a) as a function of composition; the error bars span the range of values determined from the two decomposition methods. The coherent emission is essentially zero until $x \sim 0.2-0.25$, at which point it grows rapidly to a finite value. Thereafter, it remains constant, or increases slightly, until $x \sim 0.5$. [We believe that the very small intensities near E_F , evident in Fig. 5(a) for some insulating compositions, are due to factors such as control of sample stoichiometry and surface preparation.] For $x > 0.5$, there is a monotonic decrease in the coherent contribution as the number of holes in the 3*d* band increases.

An alternative manner of displaying these results is provided in Fig. 5(b), where the ratio of the coherent intensity to the total intensity $I_{\text{coh}}/I_{\text{tot}}$ versus x is plotted.

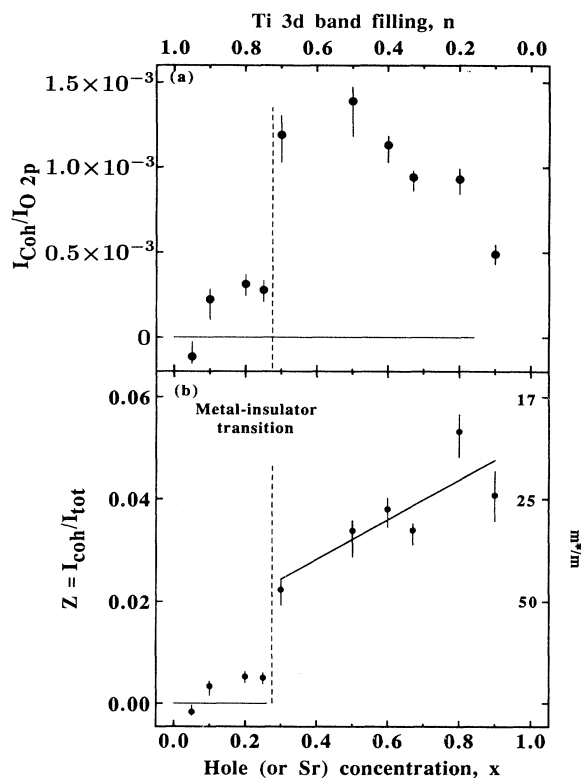


FIG. 5. (a) The coherent intensity I_{coh} in the Ti 3d spectral function (normalized to the total O 2p intensity) as a function of hole doping or Sr fraction x . The dashed line indicates the composition at the metal-insulator transition. (b) The ratio $I_{\text{coh}}/I_{\text{tot}}$, where $I_{\text{tot}} = I_{\text{coh}} + I_{\text{incoh}}$, vs hole doping. The right-hand ordinate gives the corresponding values for the effective-mass ratio, $m^*/m = 1/Z$, within the approximation discussed in the text.

(The reason for this method of presentation will be discussed below.) As for the coherent intensity alone, this ratio is either zero or very small until the composition of the bulk metal-insulator transition is reached, whereupon it increases rapidly over a very narrow composition range; the change from essentially zero to a finite value occurs for a change in band filling $\Delta x \sim 0.05$. Above the metal-insulator transition $I_{\text{coh}}/I_{\text{tot}}$ changes much more slowly, increasing by about a factor of 2 (quasilinearly) for a range $\Delta x \sim 0.65$. The most interesting point to stress is that intensity associated with the coherent intensity close to E_F clearly *does not exhibit the linear correlation with x* that is observed for the total Ti 3d emission shown in Fig. 3.

C. Spectral changes in the Ti-O hybridization region

The third effect evident in Fig. 2 is the systematic change in spectral shape of the O 2p valence structure with composition. The higher binding-energy region of the O 2p band (7–10 eV in Fig. 1) contains the majority of the hybridization between the O and Ti orbitals.^{16,17} The lower binding-energy region of the O 2p band (4–6

eV in Fig. 1) is comprised primarily of nonbonding O 2p orbitals directed between Ti cations. As x increases from 0 to ~ 0.60 , there is a shift of intensity from the region of primarily O 2p nonbonding states (lower binding energy) to the Ti 3d–O 2p bonding regions at higher binding energy, indicating a change in the Ti 3d–O 2p hybridization with composition (and band filling). For $x = 0.60$ –1.0 the spectra essentially overlap, indicating that there are no significant modifications to the Ti–O bonding for this range of composition.

As a means of illustrating the composition dependence more clearly, the O 2p valence-band regions of the spectra were fitted to the sum of two Gaussians, to represent bonding and nonbonding components, whose energy separation and widths were fixed but whose amplitudes were allowed to vary. The energy separation and widths were first determined by unconstrained least-squares fits for each of the compositions separately; the mean values of the widths and separation so determined were then fixed and used to systematically refit all the spectra. This procedure gave excellent fits to all of the $h\nu = 48$ eV spectra. The resultant bonding/nonbonding ratio is plotted in Fig. 6. (This procedure is meant to provide a means of illustrating the trend with composition, but should not be interpreted as producing the actual fraction of bonding to nonbonding states. Other procedures, such as taking

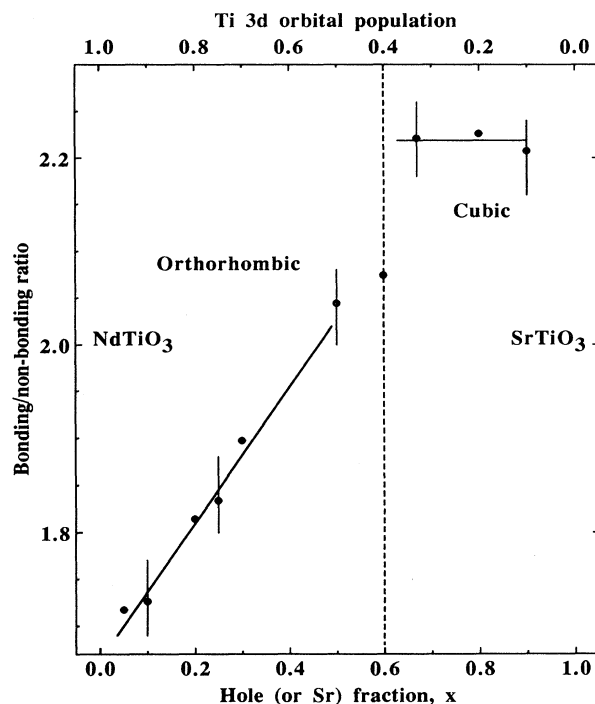


FIG. 6. The bonding/nonbonding ratio determined as described in the text vs hole doping or Sr fraction x . Conservative error bars estimated for the formation of this ratio are included for several data points. The dashed line indicates approximately where extra, weak x-ray-diffraction features indicative of the orthorhombic structure disappear with increasing x . Thereafter ($x > 0.60$) only lines indicative of the cubic perovskite structure are observed.

differences, produce the same qualitative trend.) The ratio in Fig. 6 is plotted as a function of hole doping or Sr composition on the bottom axis and Ti 3*d* orbital population, $n = 1 - x$, along the top.

In contrast to the behavior of the total band-gap emission displayed in Fig. 3, the ratio in Fig. 6 exhibits a change in slope at $x \approx 0.60$. The solid lines in Fig. 6 are the average value of the ratio for $x \geq 0.60$, and a linear fit to the data for $x < 0.60$. The interesting feature is the correlation with the crystal structure determined by x-ray diffraction. X-ray-diffraction measurements showed features indicative of an orthorhombic structure, such as that characteristic of NdTiO₃, for $x = 0$ to $x \sim 0.60$.¹² In this regime, the bonding/nonbonding ratio, and thus Ti-O hybridization, increases smoothly. As indicated in Fig. 6, the point where extra diffraction lines associated with the orthorhombic symmetry disappear is the same as that at which the ratio exhibits a change in slope. Thereafter, for $x > 0.60$ to $x = 1$, the system maintains a cubic perovskite structure, with no significant change in the Ti—O bond length, and the bonding/nonbonding ratio also remains constant. Another interesting point is that there is no clear indication, in this ratio, of the metal-insulator transition at $x \sim 0.20$ – 0.25 ; the data in Fig. 6 suggest smooth and continuous behavior through this region of composition.

IV. DISCUSSION

The Ti 3*d* character acquired by O 2*p* states due to hybridization (or covalency) is well described within a one-electron picture. Similar degrees of hybridization exist in the formally d^0 insulators TiO₂, BaTiO₃, and SrTiO₃.^{16–18} The experimental Ti 3*d* partial density of states for BaTiO₃ agrees very well with calculations based on the local-density approximation, both in terms of binding energy and the degree of hybridization.¹⁹ Hybridization of the Ti 3*d* states with the O 2*p* band results in a bandwidth large enough that correlation effects are relatively unimportant. However, the intensity closer to the Fermi level is largely Ti 3*d* in character, and the amount of O 2*p* hybridization there is not significant enough to negate the effect of correlation. The dominant structure is most aptly described as the lower Hubbard band, and existing one-electron calculations do not adequately reproduce it.^{2,11} The composition dependence in these two regions will be discussed, starting with the changes in the Ti-O hybridization revealed in Fig. 6.

The trend in Ti 3*d*–O 2*d* hybridization illustrated in Fig. 6 can be explained by considering the change in crystal structure as a function of x . In the cubic perovskite structure appropriate for $x = 1$ to $x \sim 0.6$ – 0.7 , the Ti—O—Ti bond angle is 180°. The Ti—O bond length is ~ 0.195 nm. The TiO₆ octahedra in the orthorhombic structure exhibited by NdTiO₃ are rotated to form Ti—O—Ti bond angles of 155°, and the Ti—O bond lengths are ~ 0.203 nm. Complete structure determinations are not available for all compositions, but it is generally assumed that bond angles and bond lengths vary continuously for $x < 0.60$ – 0.70 .¹²

To first order, the bond angle changes are driven by the

distortion resulting from the size difference between the Sr²⁺ and Nd³⁺ cations. The change in band filling will influence the bond length, with a larger formal valence (Ti⁴⁺ compared to Ti³⁺) resulting in a shorter bond length.¹² The correlation between changes in Ti 3*d*–O 2*p* hybridization and changes in the x-ray-diffraction features suggests that the most significant influence is the change from cubic to orthorhombic symmetry. Experimentally, the observed changes appear to be on the order of ~ 10 – 20 % of the Ti 3*d* contribution in the Ti—O bonding region [the intensity in this region in the difference curve of Fig. 1(b)]. The increase in the Ti—O bond length from SrTiO₃ to NdTiO₃ due to the change in formal valence would also reduce the Ti-O hybridization, but this would presumably be a continuous function of composition and band filling, and therefore would not explain the change in slope at $x \sim 0.60$. The two effects must, of course, operate synergistically to produce the final structure.

The behavior of the total intensity from the predominantly Ti 3*d* states near E_F (Fig. 3) indicates that the filling of the conduction bands is proportional to the Nd concentration, as expected. A discussion of the changes in the spectral shape in this region, however, requires a framework beyond a simple one-electron densities-of-states picture. The more appropriate concept of the one-electron spectral function has already been introduced. We note that the behavior exhibited in Fig. 5(a) for the coherent intensity is very similar to that observed for the effective number of electrons contributing to the Drude response in Y_{1-x}Ca_xTiO₃, determined from the optical measurements of Taguchi *et al.*,²⁰ although the result in Fig. 5 shows a much more abrupt increase at the metal-insulator composition. This similarity in behavior is in agreement with the expectation that this intensity is associated with the one-electron-like, nearly free-carrier contribution.

The rationale for plotting the ratio $I_{\text{coh}}/I_{\text{tot}}$ in Fig. 5(b) lies in its identification with the quasiparticle renormalization constant, usually denoted as Z .¹ This ratio gives the fraction of the excitation that can be identified with a well-defined quasiparticle. With some assumptions, to be discussed below, Z can also be used to make connection to the effective-mass ratio, m^*/m .²¹ The relative intensities in the coherent and incoherent contributions depend on the importance of correlation effects. The importance of correlation, in turn, will depend primarily on the band filling and the ratio U/W . It is clear that the Ti 3*d* band filling is changing, but the results above indicate that the Ti-O hybridization is also changing. A decrease in the Ti-O hybridization (with decreasing x) will lead to a reduced bandwidth W for states with Ti—O bonding character. Thus, to the extent that the low-lying Ti 3*d* conduction states are composed of Ti-O hybrids, they too will have a reduced bandwidth with decreasing hole doping.

Some theoretical examinations of the influence of either U/W or band filling on Z , or related quantities, are available, although none are completely applicable because they tend to be based on Hubbard-type models, which produce insulating behavior only in the case of in-

teger band filling. This condition is clearly not met here because the metal-insulator transition occurs for a hole concentration of $x \sim 0.25$, but it is still useful to mention briefly some results. The original treatment of Hubbard²² described a situation where the splitting between the upper and lower Hubbard bands decreases as U/W becomes small. A metal-insulator transition (Mott-Hubbard transition), which in that case is essentially a band-crossing transition, occurs when the two Hubbard bands overlap. Mott²³ suggested that the transition is discontinuous in U/W . We might then also expect the coherent intensity (and Z) to exhibit discontinuous behavior at the transition. The behavior of Z with doping was studied by Jarrel and Pruschke,²⁴ employing an infinite dimensional extension of the Hubbard model.²⁵ That treatment seemed to indicate a quasilinear increase in Z away from integer band filling. Other related model calculations produce similar dependencies.²⁶

Thus the most interesting aspect of the data in Fig. 5 is the rapid appearance of the coherent intensity at the composition of the metal-insulator transition. The transition from essentially zero coherent intensity to a finite value occurs over a very small range of both band filling ($\delta x \sim 0.05$) and bandwidth. Although we cannot separate the Ti-O bandwidth, if we assume that $W \sim 1-2$ eV,¹¹ and that the change in W across the whole composition range is approximately $\sim 10-20\%$, based on the change in the Ti-O-Ti bond angle, then the region near the metal-insulator transition over which there is a significant increase in I_{coh} corresponds to a change $\delta W/W$ on the order of 1%. The ratio U/W could also change due to a variation in U with composition, but we do not expect U to vary significantly. We also note that both the band filling and hybridization appear to vary smoothly through the composition range of the metal-insulator transition (Figs. 3 and 6). It is, however, difficult to use our results to make detailed connections to the theoretical models mentioned above because of the previously mentioned inadequacy of Hubbard-based models. Other factors, possibly disorder or other extensions to the Hubbard treatment, must be considered.

It is also useful to compare our results with the work of Inoue *et al.*,¹¹ who studied the dependence of the $3d$ spectral function on bandwidth in $\text{Ca}_{1-x}\text{Sr}_x\text{VO}_3$. In that system, the structural modifications are similar to those exhibited by $\text{Nd}_{1-x}\text{Sr}_x\text{TiO}_3$, but there is presumably no change in the Ti $3d$ band occupation; the formal valence is d^1 for all compositions. The primary structural modification is from a $V-O-V$ bond angle of 180° in SrVO_3 to an angle of $\sim 160^\circ$ in CaVO_3 . Thus the fractional change in the metal $3d$ -O $2p$ hybridization across the composition range is expected to be roughly the same as in $\text{Nd}_{1-x}\text{Sr}_x\text{TiO}_3$. We cannot compare the behavior across the metal-insulator transition because there is no such transition in $\text{Ca}_{1-x}\text{Sr}_x\text{VO}_3$. However, CaVO_3 is claimed to be close to a metal-insulator transition, requiring only a very slight ($\sim 1\%$) overoxidation to become insulating.¹¹ Therefore, a rather abrupt loss of coherent intensity over a small range of band filling should also occur in this system, because there is still significant coherent intensity in the CaVO_3 spectrum of Ref. 11. It

is also interesting to compare the gradual increase in Z for metallic compositions away from the transition in $\text{Nd}_{1-x}\text{Sr}_x\text{TiO}_3$ with the behavior observed in $\text{Ca}_{1-x}\text{Sr}_x\text{VO}_3$. The ratio of $I_{\text{coh}}/(I_{\text{coh}}+I_{\text{incoh}})$ for $\text{Ca}_{1-x}\text{Sr}_x\text{VO}$ varies quasilinearly from ~ 0.05 (CaVO_3) to ~ 0.2 (SrVO_3), compared with a variation from ~ 0.025 just above the metal-insulator transition in $\text{Nd}_{1-x}\text{Sr}_x\text{TiO}_3$ ($x=0.25$), to ~ 0.05 close to SrTiO_3 . The larger variation in $\text{Ca}_{1-x}\text{Sr}_x\text{VO}_3$ indicates that the influence of the change in bandwidth must be larger in that case.

As a final point, we consider comparisons in terms of the effective mass for carriers in the Ti $3d$ bands. With the simplifying assumption of a k -independent self-energy, i.e., $\Sigma(k,E) \sim \Sigma(E)$, the effective-mass ratio can be related to Z by $m^*/m = 1/Z$.^{1,21} The results in Fig. 5 then indicate a divergence in m^* on approaching the transition from the metallic side. Analysis of optical and transport data to determine effective-mass values for similar systems have also indicated similar behavior, with mass enhancements at the metal-insulator transition.^{20,27-29} The values reported for the effective mass in the various studies differ, however. The dominance, for all compositions, of the component attributed to incoherent intensity (producing a small value of Z) in our photoemission data suggests a large mass throughout the composition range. With the assumption above concerning the self-energy, m^*/m varies in the metallic regime from about 20 for Sr-rich compositions to about 40 close to the metal-insulator transition. The appropriate values of m^*/m are provided on the right-hand ordinate of Fig. 5(b). Comparison transport studies indicated values of $m^*/m \sim 10-20$.²⁹ In contrast, values from optical data were typically $m^*/m \sim 2-4$.^{20,27}

An interesting proposal was raised in the $\text{Ca}_{1-x}\text{Sr}_x\text{VO}_3$ investigation that may, in part, explain some of these discrepancies. The authors of Ref. 11 suggested that the assumption of a k -independent self-energy is not applicable. Using a model for the self-energy that was both energy and momentum dependent, they simulated the coherent intensity in their spectra (the incoherent intensity was not modeled) and determined $m^*/m \sim 2-4$, in agreement with spin susceptibility and electronic specific-heat data for that system. Using the assumption of a k -independent self-energy, they instead obtained values of $m^*/m \sim 45$, close to those obtained within this approximation in this study. The conclusions in Ref. 11 thus provide a consistent picture for many of the measurements of the effective mass, but more work is required to clearly determine the role (and source) of the k dependence of the self-energy in these systems.

V. SUMMARY

We have examined changes in the electronic structure that occur as a function of composition in the correlated transition-metal-oxide system $\text{Nd}_{1-x}\text{Sr}_x\text{TiO}_3$. Changes in the degree of Ti-O hybridization are observed which are correlated with the change in crystal structure from cubic for SrTiO_3 to orthorhombic for NdTiO_3 . The spectral function for emission from Ti $3d$ states was decom-

posed into coherent and incoherent components, and the behavior of these across the metal-insulator transition was extracted. The coherent contribution appears abruptly at the metal-insulator composition, while changes in the Ti 3d band filling and the bandwidth W vary smoothly across the transition.

ACKNOWLEDGMENTS

We would like to thank the staff at the SURF II storage ring for their assistance. One of us (B.W.E.) would like to acknowledge the NSF for support through Grant No. DMR-9223060 and EPRI.

- ¹G. A. Sawatzky, in *High Temperature Superconductivity*, edited by D. P. Tunstall and W. Barford (Hilger, Bristol, 1991), p. 145.
- ²A. Fujimori, I. Hase, H. Namatame, Y. Fujishima, Y. Tokura, H. Eisaki, S. Uchida, K. Takegahara, and F. M. F. de Groot, *Phys. Rev. Lett.* **69**, 1796 (1992).
- ³S. W. Robey, L. T. Hudson, C. Eylem, and B. W. Eichhorn, *J. Supercond.* **7**, 917 (1994).
- ⁴R. G. Egdell, M. R. Harrison, M. D. Hill, L. Porte, and G. Wall, *J. Phys. C* **17**, 2889 (1984).
- ⁵A. Chainani, M. Mathew, and D. D. Sarma, *Phys. Rev. B* **46**, 9976 (1992).
- ⁶D. D. Sarma, A. Chainani, R. Cimino, P. Sen, C. Carbone, M. Mathew, and W. Gudat, *Europhys. Lett.* **19**, 513 (1992).
- ⁷D. D. Sarma, O. Rader, T. Kachel, A. Chainani, M. Mathew, K. Hollmack, W. Gudat, and W. Eberhardt, *Phys. Rev. B* **49**, 14 238 (1994).
- ⁸A. Chainani, M. Mathew, and D. D. Sarma, *Phys. Rev. B* **47**, 15 397 (1993).
- ⁹A. Chainani, M. Mathew, and D. D. Sarma, *Phys. Rev. B* **48**, 14 818 (1993).
- ¹⁰A. Fujimori, I. Hase, M. Nakamura, H. Namatame, Y. Fujishima, Y. Tokura, M. Abbate, F. M. F. de Geoot, M. T. Czyzyk, J. C. Fuggle, O. Strebel, F. Lopez, M. Domke, and G. Kaindl, *Phys. Rev. B* **46**, 9841 (1992).
- ¹¹I. H. Inoue, I. Hase, Y. Aiura, A. Fujimori, Y. Haruyama, T. Maruyama, and Y. Nishihara, *Phys. Rev. Lett.* **74**, 2539 (1995).
- ¹²C. Eylem, H. L. Ju, B. W. Eichorn, and R. L. Greene, *J. Solid State Chem.* **114**, 164 (1995).
- ¹³S. W. Robey, L. T. Hudson, C. Eylem, and B. Eichorn, *Phys. Rev. B* **48**, 562 (1993).
- ¹⁴L. C. Davis, *J. Appl. Phys.* **59**, R25 (1986).
- ¹⁵X. Li, Z. Zhang, and V. E. Henrich, *J. Electron Spectrosc.* **63**, 253 (1993).
- ¹⁶Z. Zhang, S. Jeng, and V. Henrich, *Phys. Rev. B* **43**, 12 004 (1991).
- ¹⁷L. T. Hudson, R. L. Kurtz, S. W. Robey, D. Temple, and R. L. Stockbauer, *Phys. Rev. B* **47**, 1174 (1993).
- ¹⁸N. B. Brookes, D. S.-L. Law, T. S. Padmore, D. R. Warburton, and G. Thornton, *Solid State Commun.* **57**, 473 (1986).
- ¹⁹S. W. Robey, L. T. Hudson, V. E. Henrich, C. Eylem, B. Eichhorn, *J. Phys. Chem. Solids* (to be published).
- ²⁰Y. Taguchi, Y. Yokura, T. Arima, and F. Inaba, *Phys. Rev. B* **48**, 511 (1993).
- ²¹G. D. Mahan, in *Many-Particle Physics* (Plenum, New York, 1981), p. 475.
- ²²J. Hubbard, *Proc. R. Soc. London, Ser. A* **281**, 401 (1964).
- ²³N. F. Mott, in *Metal-Insulator Transitions* (Taylor & Francis, London, 1990), Chap. 4.
- ²⁴M. Jarrell and Th. Pruschke, *Z. Phys. B* **90**, 187 (1993).
- ²⁵W. Metzner and D. Vollhardt, *Phys. Rev. Lett.* **62**, 324 (1989); E. Muller-Hartmann, *Z. Phys. B* **74**, 507 (1989).
- ²⁶C. A. R. Sa de Melo and S. Doniach, *Phys. Rev. B* **41**, 6633 (1990).
- ²⁷Y. Fujishima, Yu. Tokura, T. Arima, and S. Uchida, *Physica C* **185-189**, 1001 (1991).
- ²⁸Y. Tokura, Y. Taguchi, Y. Okada, Y. Fujishima, T. Arima, K. Kumagai, and Y. Iye, *Phys. Rev. Lett.* **70**, 2126 (1993).
- ²⁹H. L. Ju, C. Eylem, J.-L. Peng, B. W. Eichhorn, and R. L. Greene, *Phys. Rev. B* **49**, 13 335 (1994).